Toward Macroscale, Isotropic Carbons with Graphene-Sheet-Like Electrical and Mechanical Properties

Marcus A. Worsley, Supakit Charnvanichborikarn, Elizabeth Montalvo, Swanee J. Shin, Elijah D. Tylski, James P. Lewicki, Art J. Nelson, Joe H. Satcher Jr., Juergen Biener, Theodore F. Baumann, and Sergei O. Kucheyev*

Realization of macroscale three-dimensional isotropic carbons that retain the exceptional electrical and mechanical properties of graphene sheets remains a challenge. Here, a method for fabricating graphene-derived carbons (GDCs) with isotropic properties approaching those of individual graphene sheets is reported. This synthesis scheme relies on direct cross-linking of graphene sheets via the functional groups in graphene oxide to maximize electronic transport and mechanical reinforcement between sheets and the partial restacking of the sheets to increase the material density to about 1 g cm^{-3}. These GDCs exhibit properties 3–6 orders of magnitude higher than previously reported 3D graphene assemblies.

1. Introduction

Individual graphene sheets have attracted a lot of attention since their isolation by Novoselov et al. [1] due to the multitude of graphene's exceptional properties.[2–10] Some of the properties observed in this nanoscale, two-dimensional (2D) form of graphitic carbon include room-temperature electrical conductivities up to ~10^6 S cm^{-1} and Young's moduli up to ~10^6 MPa, which are among the highest reported for any material. In an effort to realize the properties of individual graphene sheets on the macroscale, several groups have recently developed three dimensional (3D) graphene assemblies with many promising characteristics.[11–25] Such assemblies are comprised of randomly interconnected graphene sheets with a large degree of porosity (>90%), which is believed to be necessary to minimize restacking of graphene sheets. These low-density nanoporous graphene structures exhibit electrical conductivities and Young's moduli as many as 10 orders of magnitude lower than those observed for individual graphene sheets, which is not surprising given their high porosity. It is a direct consequence of superlinear dependences of electrical and mechanical properties on the monolith density for porous materials.[26–29] A recent attempt to address this with higher density assemblies has resulted in improvements in some mechanical properties, but the electrical conductivity has remained relatively low and comparable to that of low-density counterparts.[12] Therefore, macroscale 3D graphene-based materials exhibiting the exceptional properties of graphene sheets are a significant challenge.

Here, we report a straightforward and relatively low-temperature method to realize macroscopic 3D graphene-derived carbons (GDC) with isotropic properties approaching those of graphene sheets. Essential elements to assembling a macrostructure with such properties are i) the development of strong covalent links between graphene sheets that facilitate both electrical conductivity and structural reinforcement, ii) sufficient restacking of graphene sheets to reach relatively high densities of ≈1 g cm^{-3}, and iii) an assembly that can be carbonized at relatively low temperatures (≈1000 °C). In order to form strong links between graphene sheets in GDCs, the present method is based on chemical cross-linking of individual sheets of graphene oxide (GO) suspended in water. Such cross-linking involves various GO functional groups (e.g., epoxide and hydroxide), yielding a reduced GO gel. Upon annealing at about 1000 °C the organic cross-links are reduced to sp^2 carbon cross-links. This approach was recently demonstrated in the synthesis of exceptionally stiff and electrically conductive low-density graphene macroassemblies (GMAs).[18] The restacking of graphene sheets in the GDC is achieved by simply drying the reduced GO gel under ambient conditions instead of using a supercritical solvent extraction method that preserves the low-density structure and minimizes sheet restacking in GMAs. The dried monoliths are then annealed to produce sp^2 carbon cross-links. Resultant GDCs display isotropic bulk properties such as electrical conductivities and Young's moduli that are 3–6 orders of magnitude higher than for any previously reported 3D graphene assembly as well as exceeding the properties of isotropic graphite [30–32] that is nearly twice as dense.

2. Results and Discussion

Synthesis of GDCs was carried out via gelation of a GO suspension under basic conditions. Full experimental details are

Dr. M. A. Worsley, Dr. S. Charnvanichborikarn, Dr. E. Montalvo, Dr. S. J. Shin, E. D. Tylski, Dr. J. P. Lewicki, Dr. A. J. Nelson, Dr. J. H. Satcher Jr., Dr. J. Biener, Dr. T. F. Baumann, Dr. S. O. Kucheyev
Lawrence Livermore National Laboratory
Physical and Life Sciences Directorate
7000 East Avenue, Livermore, CA 94550, USA
E-mail: worsley1@llnl.gov

DOI: 10.1002/adfm.201400316

available in the Supplementary Materials. Briefly, in a typical synthesis, ultrasonication is used to disperse 2 wt% GO in deionized water. Concentrated NH_4OH is added (211 μL g^{-1} GO suspension) to the suspension, which is then sealed and placed in an oven at 85 °C to gel. After gelation, the reduced GO gel is washed first in deionized water and then in acetone. After that, the gel is allowed to dry under ambient conditions for at least 24 h, followed by annealing at 1050 °C under nitrogen to yield the final GDC with a monolith density of ≈1 g cm^{-3}. This is a ≈10-fold increase in the density compared to GMAs that have densities of ≈0.10 g cm^{-3}. Most importantly, the randomly orientated self-assembly during gelation combined with the capillary force-induced shrinkage lead to the formation of a completely isotropic material. **Figure 1**a shows monoliths immediately after gelation, after supercritical drying, and after ambient drying to illustrate the shrinkage that occurs upon solvent removal. There are few limits on the shapes and sizes of the GDCs produced since, in addition to being readily mechanically machined (Figure 1a, inset), the GDC conforms to the mold in which the initial reaction mixture is placed.

A large difference in the microstructure of GDCs and GMAs is illustrated by scanning electron microscopy (SEM) images in Figure 1. GMAs are made of randomly interconnected graphene sheets with a minimal restacking (Figure 1b,c) resulting in fine sheet-like features and a large porosity of ≈95%.[11,14,16–20,22] In contrast, no fine sheet-like features are distinguishable in the GDC in Figure 1d,e. The SEM shows that the GDC is homogenous and contains much less porosity than the GMA. This lower porosity contributes to the material's density being roughly half of the density for single crystalline graphite made of perfectly stacked graphene sheets (2.2 g cm^{-3}) compared to the ultralow density GMA. This apparent porosity of the GDC is consistent with the measured Brunauer-Emmett-Teller (BET) surface area of 69 m^2 g^{-1} determined by nitrogen porosimetry.

Transmission electron microscopy (TEM) gives further details concerning the sheet assembly in the GDC and illustrates one of the key differences between the GDC and graphite: the use of chemical cross-linking versus Van der Waals (VdW) forces to govern sheet-to-sheet interactions. The TEM images of commercial graphite show large domains of highly ordered, perfectly stacked graphene sheets. (Figure 1f) This perfect stacking is only possible if the sheets are loosely associated with each other (VdW) and are able to slide until this final configuration is achieved. In contrast, no regimes of perfectly stacked graphene sheets are observed in the GDC. (Figure 1g,h) The sheets are closely associated with each other, but possess a spectrum of curvature and orientations. We suggest that this imperfect or partial stacking is due to the fact that, like the GMA, the graphene sheets are cross-linked at various points by sp^2 carbon bonds.[18,33] (an assertion that is further confirmed by solid state NMR analysis, see **Figure 2**) These strong chemical cross-links make it impossible for the sheets to slide into the perfectly stacked layers observed in graphite. The incomplete stacking also contributes to the lower density of the GDC compared to commercial graphite.

From the ^1H & ^{13}C NMR data in Figure 2 it can be observed that the GO powder has a number of chemically distinct populations of carbon and hydrogen. Consistent with the known structure of GO,[18] sp^2 hybridized carbon (≈121 ppm) makes up the majority of the observed ^{13}C signal which correlates

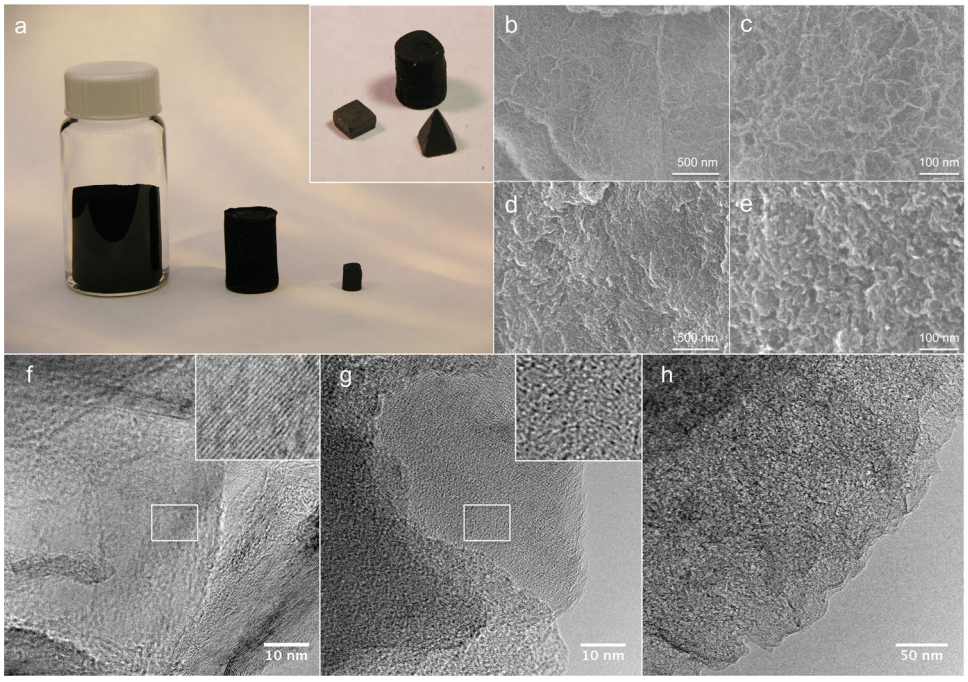

Figure 1. a) Photograph of a reduced GO wet gel before drying (left), after supercritical drying (middle), and after ambient drying (right). For reference, the wet gel is in a 20 ml vial. Inset shows a GDC cylinder (cast), prism (machined), and pyramid (machined). SEM images of fracture surfaces of b,c) the GMA and d,e) GDC at b,d) low and c,e) high magnification. f) TEM images of commercial graphite at high magnification. Inset is a zoom-in of white box area and is 10 nm in width. g) TEM image of GDC at high magnification. Inset is a zoom-in of white box area and is 10 nm in width. h) Low magnification TEM image of GDC.

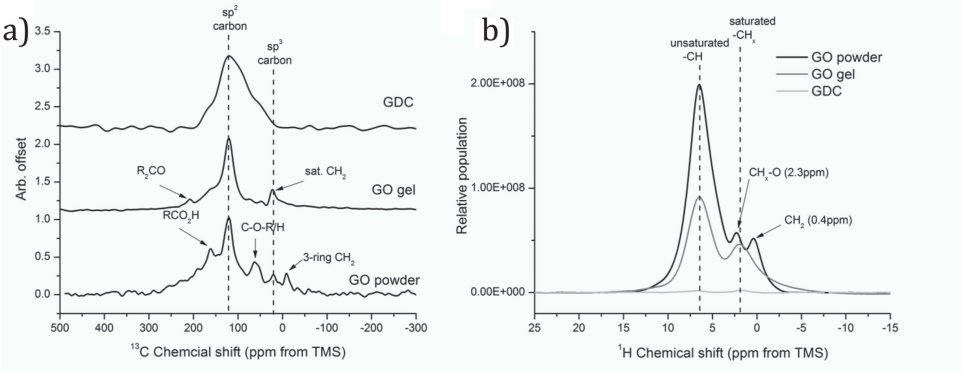

Figure 2. Solid-state ^{1}H and ^{13}C spectra of GO powder, GO gel, and annealed GDC. a) Normalized ^{13}C spectra of all three systems showing the rich structural diversity of the GO powder, the loss of epoxy, carboxyl and alcohol functionality on gelation and the final inorganic carbon matrix of the GDC which has a single, broad sp^2 hybridized population of carbon. b) ^{1}H spectra (actual scale) showing three distinct populations of protons in the GO samples, the loss of some structural diversity on gelation and an extremely small residual proton population in the final GDC structure.

with the large unsaturated CH peak in the proton spectrum of the GO powder. In the GO powder we also observe epoxy/hydroxyl functionality at ≈63 ppm and carboxyl groups at ≈161 ppm, consistent with the general structure of GO. In the ^{13}C spectrum we also observe a small signal at –8 ppm, which corresponds with a 3-ring cycloalkane structure. . On gelation, we observe the loss of epoxy, hydroxyl and carboxylic functionalities and the in-growth of sp^3 hybridized saturated CH_2 and ketone populations at 23 and 209 ppm, respectively. These peaks correspond to the cross-links (–CH_2– and –C(= O)–) formed on gelation of the structure. After the thermal anneal, only one broad population of carbon can be observed in the ^{13}C spectrum at ≈121 ppm, which corresponds to the highly rigid, sp^2 hybridized structural carbon of the GDC matrix. The ^{1}H NMR spectrum of GDC confirms that the sp^3 hybridized cross-links of the gel have been converted to sp^2 carbon cross-links, as evidenced by a very small residual population of organic hydrogen present in the GDC.

The x-ray diffraction (XRD) patterns for GDCs and GMAs also show significant deviations (**Figure 3**a). The appearance of peaks at ≈12°and 26.5° for the GDC contrasts sharply with their absence in the low-density analog. For the GMA, XRD reveals that only single and few-layer sheets exist,[18] evidenced by the absence of the (002) diffraction peak (at 26.5°) assigned to the basal spacing of graphite (0.35 nm). However, the GDC shows a strong (002) peak at 26.5°, indicating significant graphene sheet restacking, which is consistent with an increased monolith density, though the broadness of the peak suggests more disorder than observed in commercial graphite. We attribute this disorder to incomplete and imperfect restacking caused by random orientation and curvature of graphene sheets, resulting from our sheet-to-sheet cross-linking scheme. It is assumed that this imperfect stacking further contributes to the lower (relative to graphite) GDC density of ≈1 g cm^{-3}.

The Raman spectra (Figure 3b) provide more evidence for incomplete and imperfect restacking of the graphene sheets. In comparison with the highly oriented pyrolytic graphite (HOPG) and commercial graphite, which possess narrow D and G bands (G only for HOPG) and well-defined second order (D' and G') bands due to high degrees of crystallinity and ordering among sheets,[34,35] the Raman spectra for GDC serves as a sharp contrast. The D and G bands for the GDC are fairly broad and the second order peaks are almost indistinguishable. In fact the Raman spectra for the GDC is strikingly similar to that of the GMA, indicative of the random orientation and curvature of the graphene sheets due to the sheet-to-sheet cross-linking scheme, even at ≈10 times the density.[18,33] Also, like the GMA, the GDC showed an extremely low oxygen content, determined to be less than 2 at% by EDX (Figure S1, Supporting Information) and 4 at% by RBS and XPS (Table S1, Supporting Information). This is much lower than the GO powder (20–25 at%) and quite similar to the GMA (2 at%). Furthermore, it was extremely thermally stable, losing less than 1% mass up to 1000 °C under nitrogen (Figure S2, Supporting Information).

Despite having a density of close to half of that of perfectly stacked graphene sheets (2.2 g cm^{-3}) or even commercial grade graphite (1.6–1.9 g cm^{-3}), the mechanical properties of the GDC (randomly stacked, cross-linked sheets) exceed those of graphite. Nanoindentation results (Figure 3c) show that the GDC exhibits a Young's modulus of ≈10 GPa and a failure stress of ≈1.2 GPa independent of the loading direction. These exceed respective nanoindentation values of 8.5 GPa and 0.4 GPa (also independent of loading direction) for commercial grade graphite[30] with a much larger density of 1.7 g cm^{-3}. Uniaxial compression results also show that the GDC has a high compressive strength of ≈200 MPa compared to only ≈98 MPa for the commercial graphite material (Figure 3d). The measured compressive strength for commercial graphite is consistent with reported values of 40–193 MPa, depending on the material density (1.6–1.9 g cm^{-3}) and defect content.[30–32] The much-improved mechanical properties of the GDC can be attributed to its unique nanostructure. As seen in the TEM images, though there is significant restacking of the graphene sheets, there is no preferred orientation, resulting in isotropic mechanical response. Furthermore, instead of relying on weak VdW forces between sheets as in commercial graphite, the GDC graphene sheets are cross-linked with strong sp^2 bonds. These chemical cross-links allow for much stronger structural reinforcement between graphene sheets than found in traditional graphite.

Considering that Young's modulus depends superlinearly on monolith density, ρ, for nanoporous materials with

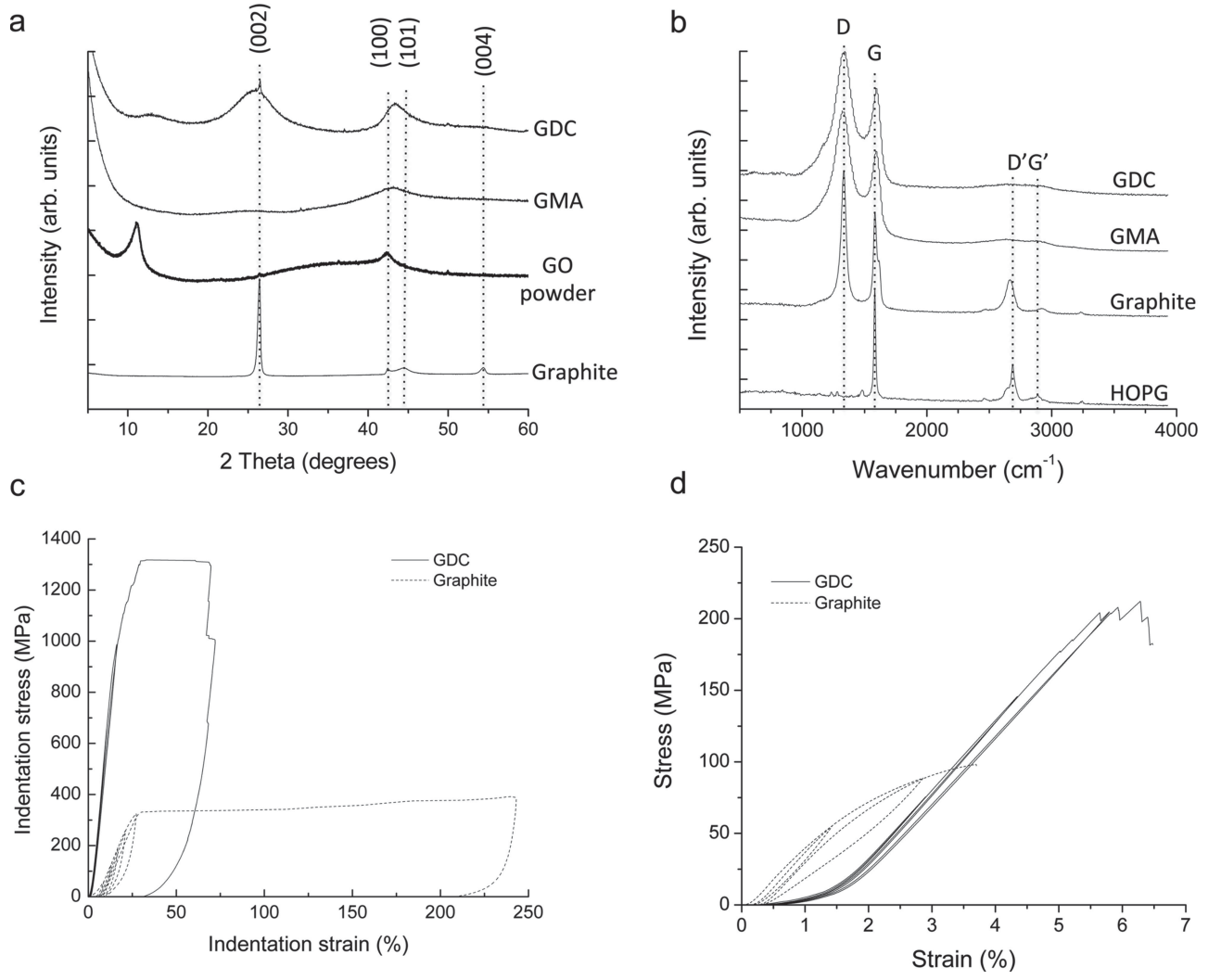

Figure 3. a) XRD spectra for GDC, GMA, GO powder and commercial graphite. b) Raman spectra for GDC, GMA, commercial graphite, and highly oriented pyrolytic graphite (HOPG). c) Nanoindentation stress vs strain plot for GDC and graphite. d) Macroscale uniaxial compression stress vs strain plot for the GDC and graphite.

an exponent, *n*, in the range of 2–4, **Figure 4**a shows a density dependence of the modulus for a number of carbon materials, including carbon aerogels,[27] carbon-nanotube (CNT) assemblies[29], graphene,[4,10] graphene-based materials,[18,36,37] and graphite.[30–32] Figure 4a shows that the modulus of the GDC scales with density as expected for CNT- or

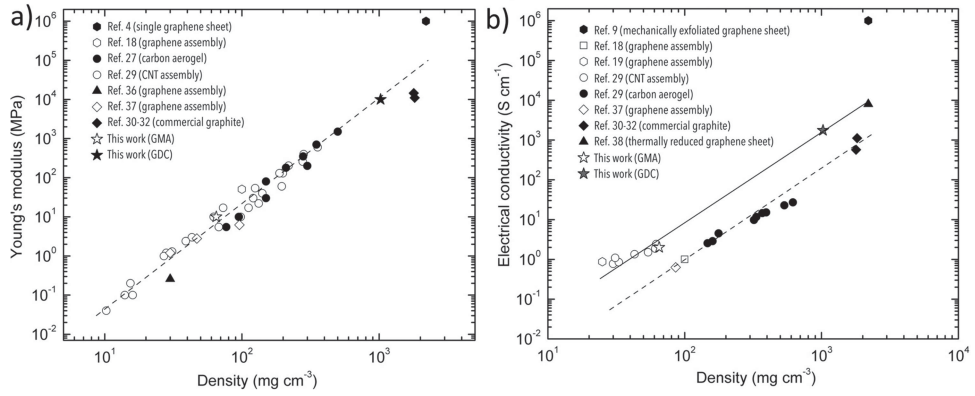

Figure 4. Log–log plot of a) Young's modulus and b) electrical conductivity as a function of density.

graphene-based materials with $n = 2.5$. In fact, Figure 4a suggests that if the density of the GDC could be further increased to ≈2 g cm^{-3}, the modulus would come within an order of magnitude of that for an individual atomically perfect graphene sheet (10^6 MPa). The scaling of the modulus to a value lower than that of an atomically perfect graphene sheet probably stems from random orientation and curvature of graphene sheets as well as lattice defects. Nevertheless, it is quite remarkable that the GDC exhibits properties so close to those expected based on the density scaling of an assembly of atomically perfect graphene sheets.

The bulk electrical conductivity of the GDC, determined via the four-probe method, is 1750 S cm^{-1}, independent of probe orientation, which, to our knowledge, is larger than that observed for any 3D graphene assembly reported by several orders of magnitude.[12,18] Even high density graphene assemblies that have been annealed under similar conditions exhibit far lower conductivities than the GDC.[12] Figure 4b plots the density dependence of the electrical conductivity of the GDC along with other reported 3D graphene[18,19,37] and CNT assemblies,[29] carbon aerogels,[29] graphite,[30–32] and individual graphene sheets[9,38]. Similar to the scaling of Young's modulus discussed above, electrical conductivity, σ, scales superlinearly with the material density ($\sigma \sim \rho^{1.5}$). Figure 4b shows that, despite pronounced restacking of graphene sheets revealed by an increased density and combined SEM, TEM, XRD, and BET observations, the GDC follows the scaling law for CNT- and graphene-based materials, extrapolating to a conductivity of ≈10^4 S cm^{-1} at ≈2 g cm^{-3}. This result is approximately 2 orders of magnitude less than what is observed for a perfect graphene sheet, highlighting how sensitive the electrical conductivity is to defects, sheet curvature, sheet stacking, and orientation (in-plane vs through-plane). A scaled GDC conductivity of ~10^4 S cm^{-1} is, however, consistent with experimental conductivity values for individual graphene sheets thermally reduced from GO[38] and is an order of magnitude higher than that of commercial graphite[30–32]. This improvement in electrical conductivity, as was the case with the mechanical properties, can be attributed to the unique nanostructure of the GDC. Conductive sp^2 bonding between graphene sheets in all directions lowers the sheet-to-sheet resistance compared to traditional graphite, which is limited to higher resistance VdW sheet-to-sheet bonding.

3. Conclusion

In summary, we have presented a straightforward method to realize high-density graphene-based macroassemblies with isotropic mechanical and electronic transport properties approaching those of individual graphene sheets. Our design strategy involves direct cross-linking of graphene sheets via the functional groups in graphene oxide and sufficient restacking of the graphene sheets to increase the material density. The nature of the synthesis requires a much lower temperature than for the synthesis of commercial isotropic graphite and facilitates fabrication with few limits on the size or shape. We anticipate that the development of 3D bulk macrostructures retaining properties of individual graphene sheets will both expand and accelerate the commercialization of graphene-based technologies and products.

Supporting Information

Supporting Information is available from the Wiley Online Library or from the author.

Acknowledgements

This work was performed under the auspices of the U.S. Department of Energy by Lawrence Livermore National Laboratory under Contract DE-AC52-07NA27344. Funding was provided by the DOE Office of Energy Efficiency and Renewable Energy, and the Lawrence Livermore National Laboratory Directed Research and Development (LDRD) Grant 12-ERD-035 and 13-LW-099.

Received: January 28, 2014
Published online: April 2, 2014

[1] A. K. Geim, S. V. Morozov, D. Jiang, Y. Zhang, S. V. Dubonos, I. V. Grigorieva, A. A. Firsov , *Science* **2004**, *306*, 666.
[2] C. Gomez-Navarro, R. T. Weitz, A. M. Bittner, M. Scolari, A. Mews, M. Burghard, K. Kern , *Nano Lett.* **2007**, *7*, 3499.
[3] A. K. Geim, K. S. Novoselov, *Nat. Mater.* **2007**, *6*, 183.
[4] C. Lee, X. Wei, J. W. Kysar, J. Hone, *Science* **2008**, *321*, 385.
[5] J. R. Miller, R. A. Outlaw, B. C. Holloway, *Science* **2010**, *329*, 1637.
[6] K. S. Novoselov, Z. Jiang, Y. Zhang, S. V. Morozov, H. L. Stormer, U. Zeitler, J. C. Maan, G. S. Boebinger, P. Kim, A. K. Geim, *Science* **2007**, *315*, 1379.
[7] F. Schedin, A. K. Geim, S. V. Morozov, E. W. Hill, P. Blake, M. I. Katsnelson, K. S. Novoselov , *Nat. Mater.* **2007**, *6*, 652.
[8] Y. W. Zhu, S. Murali, W. W. Cai, X. S. Li, J. W. Suk, J. R. Potts, R. S. Ruoff , *Adv Mater* **2010**, *22*, 3906.
[9] J.-H. Chen, C. Jang, S. Xiao, M. Ishigami, M. S. Fuhrer, *Nat. Nanotechnol.* **2008**, *3*, 206.
[10] S. P. Koenig, N. G. Boddeti, M. L. Dunn, J. S. Bunch, *Nat. Nanotechnol.* **2011**, *6*, 543.
[11] H. Bai, C. Li, X. Wang, G. Shi, *J. Phys. Chem. C* **2011**, *115*, 5545.
[12] H. Bi, K. Yin, X. Xie, Y. Zhou, N. Wan, F. Xu, F. Banhart, L. Sun, R. S. Ruoff, *Adv. Mater.* **2012**, *24*, 5124.
[13] J. Biener, S. Dasgupta, L.-H. Shao, D. Wang, M. A. Worsley, A. Wittstock, J. R. I. Lee, M. M. Biener, C. A. Orme, S. O. Kucheyev, B. C. Wood, T. M. Willey, A. V. Hamza, J. Weissmueller, H. Hahn, T. F. Baumann, *Adv. Mater.* **2012**, *24*, 5083.
[14] W. Chen, L. Yan, *Nanoscale* **2011**, *3*, 3132.
[15] Y. Lin, G. J. Ehlert, C. Bukowsky, H. A. Sodano, *ACS Appl. Mater. Interfaces* **2011**, *3*, 2200.
[16] Z. Sui, X. Zhang, Y. Lei, Y. Luo, *Carbon* **2011**, *49*, 4314.
[17] J. Wang, M. Ellsworth, *ECS Trans.* **2009**, *19*, 241.
[18] M. A. Worsley, S. O. Kucheyev, H. E. Mason, M. D. Merrill, B. P. Mayer, J. Lewicki, C. A. Valdez, M. Suss, M. Stadermann, P. Pauzauskie, J. J. H. Satcher, J. Biener, T. F. Baumann, *Chem. Commun.* **2012**, *48*, 8428.
[19] M. A. Worsley, P. J. Pauzauskie, T. Y. Olson, J. Biener, J. H. Satcher, T. F. Baumann , *J. Am. Chem. Soc.* **2010**, *132*, 14067.
[20] Y. Xu, K. Sheng, C. Li, G. Shi, *ACS Nano* **2010**, *4*, 4324.
[21] X. Yang, L. Qiu, C. Cheng, Y. Wu, Z.-F. Ma, D. Li , *Angew. Chem. Int. Ed.* **2011**, *50*, 7325.

[22] S. Yin, Z. Niu, X. Chen, *Small* **2012**, *8*, 2458.
[23] Y. Zhao, J. Liu, Y. Hu, H. H. Cheng, C. G. Hu, C. C. Jiang, L. Jiang, A. Y. Cao, L. T. Qu , *Adv. Mater.* **2013**, *25*, 591.
[24] H. Sun, Z. Xu, C. Gao, *Adv. Mater.* **2013**, *25*, 2554.
[25] Z. Lin, G. H. Waller, Y. Liu, M. Liu, C.-p. Wong, *Nano Energy* **2013**, *2*, 241.
[26] J. Gross, J. Fricke, R. W. Pekala, L. W. Hrubesh, *Phys. Rev. B* **1992**, *45*, 12774.
[27] R. W. Pekala, C. T. Alviso, J. D. Lemay, *J. Non-Cryst. Solids* **1990**, *125*, 67.
[28] R. W. Pekala, C. T. Alviso, X. Lu, J. Gross, J. Fricke, *J. Non-Cryst. Solids* **1995**, *188*, 34.
[29] M. A. Worsley, S. O. Kucheyev, J. H. Satcher, A. V. Hamza, T. F. Baumann, *Appl. Phys. Lett.* **2009**, *94*, 073115.
[30] http://www.mcmaster.com/#graphite-rods/ = kkbdgu (accessed: 2013).
[31] http://www.poco.com/tabid/70/Default.aspx (accessed: 2013).
[32] http://www.roccarbon.com/content/carbon-graphite.html (accessed: 2013).
[33] M. A. Worsley, T. Y. Olson, J. R. I. Lee, T. M. Willey, M. H. Nielsen, S. K. Roberts, P. J. Pauzauskie, J. Biener, J. H. Satcher, T. F. Baumann, *J. Phys. Chem. Lett.* **2011**, *2*, 921.
[34] A. C. Ferrari, *Solid State Commun.* **2007**, *143*, 47.
[35] A. C. Ferrari, J. A. G. Robertson, *Phys. Rev. B* **2000**, *61*, 14095.
[36] Z. H. Tang, S. L. Shen, J. Zhuang, X. Wang, *Angew. Chem. Int. Ed.* **2010**, *49*, 4603.
[37] X. Zhang, Z. Sui, B. Xu, S. Yue, Y. Luo, W. Zhan and B. Liu *J. Mater. Chem.* **2011**, *21*, 6494.
[38] Z.-S. Wu, W. Ren, L. Gao, J. Zhao, Z. Chen, B. Liu, D. Tang, B. Yu, C. Jiang, H.-M. Cheng, *ACS Nano* **2009**, *3*, 411.